JOURNAL OF CATALYSIS 157, 636–644 (1995)

Crystal Phases, Defects, and Dynamics of Adsorbed Hydroxyl Groups and Water in Pure and Lanthanide-Modified Zirconia: A Neutron-Scattering Study

C.-K. Loong,* J. W. Richardson, Jr.,* and Masakuni Ozawa†

*Argonne National Laboratory, Argonne, Illinois 60439; and †Nagoya Institute of Technology, Tajimi, Gifu, 507, Japan

Received March 27, 1995; revised August 10, 1995

The role of lanthanide doping in zirconia as a means of stabilizing and promoting catalytic reactions was studied by neutron spectroscopy. The crystal structure of high-surface-area $Ln_{0.1}Zr_{0.9}O_{1.95}$ (Ln = La and Nd) powders prepared by a coprecipitation method were found to be composed of mixed phases of tetragonal and cubic symmetry, which can be stabilized over a temperature range (up to ~1000°C) pertinent to catalytic applications. A real-space correlation function, obtained from a Fourier transform of the filtered residual diffuse scattering, showed evidence of static, oxygen vacancy-induced atomic displacements along the pseudocubic ⟨111⟩ and other directions. The dynamics of hydrogen atoms associated with the surface hydroxyl groups and adsorbed water molecules on $Ln_{0.1}Zr_{0.9}O_{1.95}$ and pure ZrO_2 over a frequency range of 0–4400 cm^{-1} was investigated by neutron inelastic scattering. The stretch vibrations of surface hydroxyl groups on monoclinic ZrO_2 were found to have slightly higher frequencies than those for $Ln_{0.1}Zr_{0.9}O_{1.95}$. At a submonolayer coverage of water the O–H stretch bands broaden and shift to lower energies. At higher coverage three bands, corresponding to the O–H stretch, H–O–H bend, and librational motion of water molecules, were observed, indicating the influence of hydrogen bonding. The neutron results were compared with infrared data and *ab initio* calculations for similar zirconia systems found in the literature. © 1995 Academic Press, Inc.

I. INTRODUCTION

The catalytic functions of high-surface-area zirconia have attracted numerous investigations, both experimental and theoretical. Zirconia is an active isosynthesis catalyst which is capable of selective conversion of synthesis gas into branched hydrocarbons (1–6). It can also be used as a promoter and/or support component in automobile exhaust-emission-control catalysts to remove poisonous gases such as CO, NO_x, and hydrocarbons. High-efficiency three-way catalytic converters for automobiles are desirable in order to meet recent emission standards (7–10). A key desirable property for these catalysts is the ability in maintaining the large surface area, structural stability, and surface acidity/basicity of zirconia over the temperature range for catalytic reactions or pretreatments.

Doping lanthanides (Ln) into zirconia to form a solid solution of the Ln–Zr oxide system is an effective approach to improving stability of the catalysts at high temperatures. These mixed oxides are partially stabilized to the cubic and tetragonal phases and free from any disruptive structural transformation over a wide temperature range. In addition, the different valency of the cations (Ln^{3+} versus Zr^{4+}) results in oxygen vacancies, which may lead to effective adsorption sites and/or strong metal–support interactions (SMSI). One example is the improved durability and enhanced de-NO_x performance by using Ln–Zr oxide materials in supporting precious metals in automobile three-way catalytic converters (10).

For many reactions on ZrO_2 the surface hydroxyl groups and adsorbed water molecules play an essential role. Ekerdt and co-workers (2–5) described an isosynthesis reaction of $CO/H_2/H_2O$ over zirconia in which intermediate formate is derived from surface hydroxyl H and CO adsorbed on ZrO_2. Methoxide is subsequently formed from reduction of formate via intermediate oxymethylene. At relatively low temperatures (~125°C) methanol can be formed from a reaction of water and methoxide. They also studied the effect of Y-doping on promoting adsorption of reactants over oxygen vacancy sites on ZrO_2 surface. Furthermore, the water–gas shift reaction such as $CO + H_2O \rightarrow CO_2 + H_2$ occurring in automobile catalyst is known to be an important process in emission-control practice (11). It has been reported that CeO_2 is an effective promoter for this reaction as well as capable of oyxgen storage by the Ce ions. This resulted in an improved dynamic performance of automobile catalysis under the condition of air/fuel-ratio fluctuation in engine exhaust. Practical improvement of the dynamics and heat durability of three-way catalysts was achieved by the incorporation of solid solutions of zirconia, ceria, and other rare-earth oxides (10). Ozawa and Kimura (8) reported the preparation

0021-9517/95 $12.00

of *Ln*-modified ZrO_2 with high surface area from a coprecipitation method and the accelerating effect of CO oxidation from an Fe catalyst supported by Nd-doped ZrO_2. They also investigated the application of Ce–Zr oxide solid solution as promoters in automobile catalysts (10). In this paper we describe a neutron-scattering study of these high-surface-area zirconias, both the pure and *Ln*-modified (*Ln* = La and Nd) compounds, focusing on the crystal structure, defects, and dynamics of adsorbed hydroxyl and water species.

The nuclear scattering amplitude of neutrons scattered by an atom depends on the spin states of the atomic nucleus. For an element the scattering amplitude averaged over the distributions of nuclear spins and isotopes is called the *coherent* scattering amplitude. Neutron coherent scattering yields information concerning the atomic organization, both structural and dynamic, of the system. Unlike in X-ray scattering, the neutron-scattering amplitude of an atom does not increase monotonically with respect to the atomic number but often values for heavy and light atoms are comparable in magnitude. In the case of O and Zr the neutron coherent scattering amplitudes, $b_O = 0.5803 \times 10^{-12}$ cm and $b_{Zr} = 0.716 \times 10^{-12}$ cm, yield a structure factor for zirconia with good contrast in resolving the crystal and defects structure induced by oxygen deficiency and/or small displacements. We describe the characterization of the crystal phases and defects in La–ZrO_2, Nd–ZrO_2, and pure ZrO_2 from a neutron powder diffraction study.

Owing to the spin incoherence in neutron scattering from protons, the neutron-scattering cross section of hydrogen is predominantly *incoherent* and is more than 10 times greater than those of O and Zr (which are mainly coherent). Incoherent neutron scattering is ideal for probing the single-particle motions of protons in hydrogen-containing substances. Hydrogen motions associated with atomic migrations, lattice, and localized vibrations can be measured quantitatively without being subject to any selection rules. We present the measured hydrogen vibrational densities of states of the surface hydroxyl groups and adsorbed water molecules on the zirconia samples. The neutron spectra are compared with infrared data and theoretical calculations of similar zirconia systems from the literature

II. EXPERIMENTAL DETAILS

The lanthanide-modified zirconia powders were prepared by a coprecipitation technique described elsewhere (8). Briefly, mixtures of hydrous zirconium and lanthanides were coprecipitated from an agitated aqueous solution of $ZrOCl_2$ and $LnCl_3$ (total concentration of 0.8 mol^{-1} at the final pH value of 10) with excess of 10 wt% NH_4OH solution. The products were filtered and washed with distilled water and then dried by a supercritical technique. The dried mixtures were calcined at selected temperatures (600 and 800°C) in air. An x mol% doped sample has a nominal chemical formula of $Ln_xZr_{1-x}O_{2-0.5x}$. The preparation of high-surface-area pure ZrO_2 began from a hydrolysis of aqueous $ZrOCl_2$ solution at 100°C for 78 h. An agglomerate, formed by addition of ammonia solution, was filtered and washed by distilled water, then washed by isopropylalcohol, and dried at 60°C for 2 days. The pure ZrO_2 powder was obtained from a heat treatment of the product at 290°C in air for 3 h. The BET surface areas in units of square meters per gram determined by nitrogen adsorption at 77 K are 78 ± 0.6 (for $La_{0.1}Zr_{0.9}O_{1.95}$ heat treated at 600°C), 73 ± 0.8 ($Nd_{0.1}Zr_{0.9}O_{1.95}$ 600°C), 51 ± 0.7 ($Nd_{0.1}Zr_{0.9}O_{1.95}$ 800°C), and 106 ± 0.8 (ZrO_2 290°C).

The crystal and defects structure of the $La_{0.1}Zr_{0.9}O_{1.95}$, $Nd_{0.1}Zr_{0.9}O_{1.95}$, and pure ZrO_2 samples were investigated by neutron powder diffraction. The experiments were carried out at room temperature using the general purpose powder diffractometer (GPPD) at the Intense Pulsed Neutron Source (IPNS) of Argonne National laboratory. A powder sample was enclosed in a thin-wall vanadium can (11 mm diameter, 50 mm long). Independent time-of-flight data were recorded on eight detector banks positioned at scattering angles ranging from ±15° to ±150° (12). The diffraction profiles collected at the backscattering geometry (at a mean scattering angle of ±148°), which correspond to the highest resolution ($\Delta d/d = 0.25\%$, where d is the atomic spacing), were analyzed by the Rietveld refinement (13) and Fourier filtering analysis (14). The former is a conventional crystallographic refinement method and the latter is a means to analyze the short-range, defects-induced structure. Prior to the diffraction measurements the lanthanide-modified and pure ZrO_2 were dried by heating to 450°C in air and 250°C in vacuum, respectively.

The dynamics of adsorbed hydrogen species on zirconia was studied by inelastic-scattering experiments, which were performed using the high-resolution medium-energy chopper spectrometer (HRMECS) also at IPNS. A pulsed-neutron source like IPNS, equipped with cold moderators, provided a large flux of cold-to-epithermal neutrons that are essential in studying the low-energy lattice modes as well as the high-energy molecular vibrations. In general, the energy resolution ΔE (full width at half-maximum) of the HRMECS spectrometer varies from ~4% of the incident energy (E_0) in the elastic region to ~2% near the end of the neutron energy-loss spectrum (15). About 40 g of powder was placed inside a sealed aluminum container in the shape of a thin slab (dimension 7.5 × 100 × 2 mm^3), which was mounted to the cold plate of a closed-cycle helium refrigerator at a 45° angle with the incident neutron beam. Such a geometry minimized multiple-scattering effects. To reduce as much as possible multiple phonon scattering, the sample was cooled to 25 K. Background scattering was subtracted from the data by using an

empty-container run. Measurements of elastic incoherent scattering from a vanadium standard provided detector calibration and intensity normalization. Two incident energies, 600 and 50 meV, were used to characterize the energy spectra from 0 to 550 meV with good resolution. Measurements were made on the dry powders as well as samples containing physisorbed water by exposing the dry powders under controlled water vapor pressure inside a humidistat.

II. RESULTS AND DISCUSSION

1. Crystal and Defects Structure

Pure ZrO_2 has three polymorphs: a cubic fluorite structure (space group $Fm3m$) above 2640 K, a tetragonal structure ($P4_2/nmc$) between 1400 and 2640 K, and a monoclinic structure ($P2_1/c$) below 1400 K. The improvement of mechanical properties of zirconia by alloying with other oxides known as transformation toughening is a technologically important field in its own right (16). The modified zirconias contain mixed cubic and tetragonal (or monoclinic) phases retained metastably over a wide range of temperatures including room temperature. The microstructure of these partially stabilized zirconias depends on many parameters related to the processing methods (8, 17–19). Our main concern here is the crystal phases and defects in the heat-treated La- and Nd-modified ZrO_2 and their relation to catalytic performance.

In the present study, neutron diffraction arises predominantly from coherent scattering of the Zr and O atoms in the crystalline lattice. Incoherent scattering from the surface hydroxyl groups in the dried powders contributes to only a small isotropic background, which was removed prior to the crystal structural refinements. Figure 1 shows the observed, background-subtracted and fitted powder pattern of the $La_{0.1}Zr_{0.9}O_{1.95}$ sample, which was heat treated at 600°C. Similar patterns were also observed for the $Nd_{0.1}Zr_{0.9}O_{1.95}$ samples heated at 600 and 800°C. In general, the peak widths are considerably larger than the instrumental resolution for all the samples, indicating the presence of microstrain and small grain-size effect. A Rietveld analysis over the entire d-spacing range from 0.5 to 2.8 Å, assuming random substitution of Zr by the lanthanide atoms, resulted in the identification of mixed tetragonal and cubic phases in all samples. As seen in Fig. 1, which is typical to all samples, all the Bragg peaks and their intensities are adequately accounted for by the tetragonal and cubic two-phase structure. Since the neutron structure factor is more sensitive to oxygen atoms than that of X rays, the present neutron-diffraction data provide a more definite characterization of the metastable phases in the lanthanide-modified zirconia samples (20). Doping lanthanide modifiers in ZrO_2 helps stabilize the cubic and tetragonal phases over the temperature range of catalytic applications thereby resulting in a better thermal stability

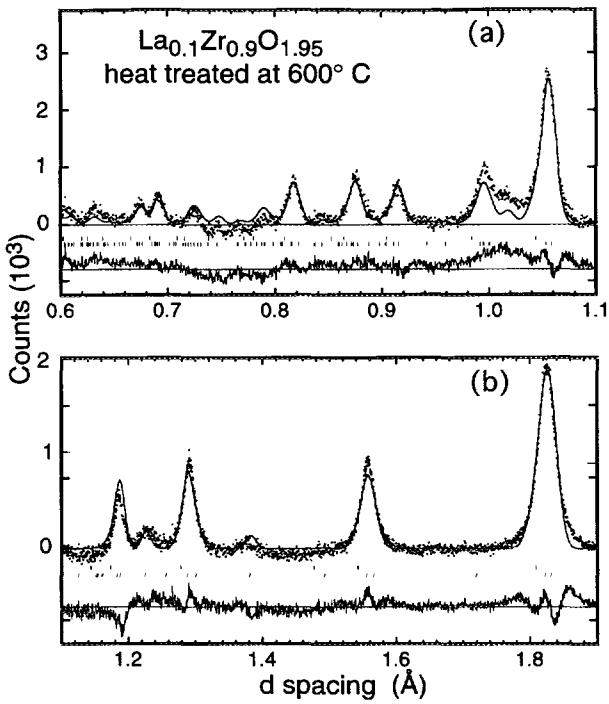

FIG. 1. Rietveld profile fit in the 0.6- to 1.9-Å region of d-spacing for the $La_{0.1}Zr_{0.9}O_{1.95}$ sample that was subjected to heat treatment at 600°C. The dots are the observed, background-subtracted intensities. The solid line represents the calculated crystalline intensities. Tick marks of the top and bottom rows indicate the positions of the Bragg reflections for the cubic and tetragonal phases, respectively. The residual intensities before Fourier filtering are shown at the bottom of the figure.

and higher resistance to sintering during the operation. However, the mechanism responsible for the removal of the disruptive tetragonal to monoclinic transformation in the present samples is believed to be different from that in the transformation-toughened zirconia ceramics such as the Y_2O_3–ZrO_2 system. In the latter materials the retention of the tetragonal crystallites is induced by the surrounding residual stress which inhibits the (diffusionless) martensitic transformation of tetragonal to monoclinic symmetry. The phase change occurs from cooperative atomic displacements without the diffusion of the cations and anions (16, 19, 20, 22, 23). In the present samples the tetragonal and cubic phases were synthesized by a low-temperature processing method of coprecipitation. The detrimental phase change at elevated temperatures of 600 to 1200°C results from decomposition by diffusion of ions followed by nucleation and crystal growth, which leads to a loss of surface area and a reduction of active sites. The larger radii and different chemical properties of the lanthanide ions from Zr play a crucial role in the suppression of the transformation and in limiting grain growth at elevated temperatures (8, 21–23).

We now discuss the defects structure associated with

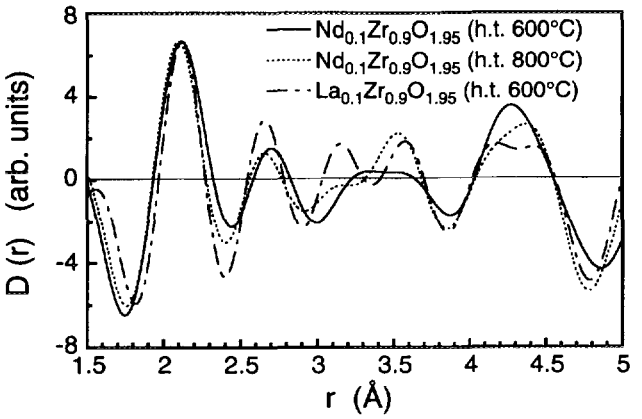

FIG. 2. Correlation function, $D(r)$, calculated from the filtered residual intensities from the Rietveld refinement of the $Ln_{0.1}Zr_{0.9}O_{1.95}$ (Ln = La and Nd) data. The features below 1.7 Å are noise due to the truncation of data.

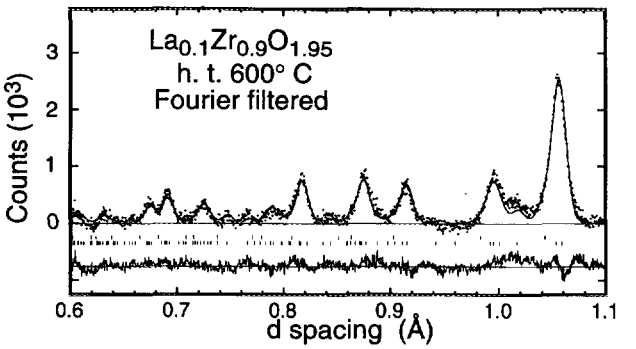

FIG. 3. Final Rietveld profile fit for the $La_{0.1}Zr_{0.9}O_{1.95}$ sample after Fourier filtering. Only the 0.6- to 1.1-Å region of d-spacing is shown.

the oxygen vacancies in the lanthanide-modified zirconias. Oxygen vacancies arise from preservation of electroneutrality in the lattice of a solid solution which mixes dopant cations (Ln^{3+}) of a lower valency than the host cations (Zr^{4+}). Composition fluctuations due to the presence of O vacancies will lead to additional diffuse-scattering components in the powder pattern. Moreover, atoms surrounding the O vacancies may relax from their lattice sites thus giving rise to further fluctuations in atomic distances. These effects manifest themselves in the diffraction pattern as broad, oscillatory deviations from the calculated crystallite profile, as evidenced in the residual intensities in Fig. 1. This residual component in the La- and Nd-doped ZrO_2 samples was analyzed by a Fourier filtering technique to extract information regarding the nature of the defects structure (14, 24). The oscillatory component was fitted by a smooth function thereby filtering out the sharp features due to the crystalline contribution. The fitted function is then Fourier transformed into the real space, yielding a correlation function, $D(r)$, similar to the radial distribution function used to describe amorphous materials. $D(r)$ displays maxima at interatomic spacings characteristic of the short-range interactions giving rise to the diffuse scattering. The $D(r)$ obtained for the three Ln–ZrO_2 samples are shown in Fig. 2. They show maxima at about 2.105 ± 0.02, 2.68 ± 0.02, 3.16 ± 0.01, 3.47 ± 0.12, and 4.35 ± 0.08 Å, which tentatively correspond to Zr–O(1), O–O(1), O–O(2); O–O(3) and Zr–Zr; and Zr–O(2) and/or O–O(4) spatial correlations, respectively. After the origin of the residual component is identified, the inverse Fourier transform of $D(r)$, truncated at an appropriate value of r_{max} = 5 Å, was subtracted from the observed data. Rietveld refinements of the resulting spectra yielded better agreement with the two-phased crystal structure (25), as illustrated by an exemplifying profile in Fig. 3 and the reasonable weighted R-factors (4.7–6.0%). A summary of the Fourier-filtered, Rietveld refinements for the three samples is given in Table 1. The microstrain and average crystallite size parameters were obtained from an analysis of the peak profiles (26, 27). The microstrain arises mainly from compositional fluctuation of Zr and dopant cations in the samples. The crystallite sizes agree with those estimated from transmission electron microscopy (8). The surface areas estimated based on these crystallite sizes are 40–50% larger than the corresponding BET surface areas. The difference is due to, presumably, agglomeration of crystallites in the powders.

The O-vacancy-induced defects in principle would add a new dimension of site selectivity in the catalytic activity in the lanthanide-modified zirconia systems. In the studies

TABLE 1

The Crystal Structure of $Ln_{0.1}Zr_{0.9}O_{1.95}$

Parameters	10 mol% Nd, 600°C	10 mol% Nd, 800°C	10 mol% La, 600°C
	Cubic $Fm3m$[a]		
a (Å)	5.1485(2)	5.1512(2)	5.1635(3)
Mole fraction (%)	58.7	54.4	53.2
Microstrain (%)	0.68(8)	0.83(9)	0.70(13)
Crystallite size (Å)	184(12)	291(56)	158(12)
	Tetragonal $P4_2/nmc$[b]		
a (Å)	3.6318(5)	3.6288(4)	3.6377(7)
c (Å)	5.2002(17)	5.1982(12)	5.2059(26)
z (O)	0.5445(5)	0.5446(5)	0.5354(7)
Mole fraction (%)	41.3	45.6	46.8
Microstrain (%)	0.95(13)	1.02(8)	1.13(18)
Crystallite size (Å)	60(2)	84(4)	54(3)
Weighted R (%)	5.9	6.0	4.7

[a] 4 Zr (a) 0, 0, 0; F. C.; 8 O (c) ± (¼, ¼, ¼); F. C.
[b] 2 Zr (a) ¾, ¼, ¾; ¼, ¾, ¼; 4 O (d) ¼, ¼, z; ¼, ¼, z + ½; ¾, ¾, −z; ¾, ¾, −z + ½.

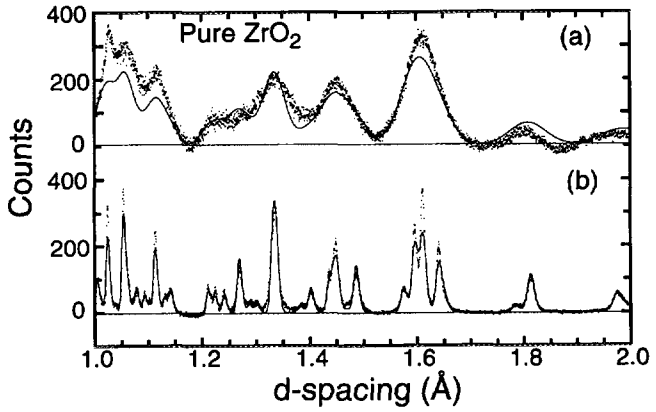

FIG. 4. Rietveld profile fit in the 1- to 2-Å region of *d*-spacing for the pure ZrO_2 sample: (a) high-surface-area powder and (b) commercial powder. The dots represent the observed, background subtracted intensities. The solid line represents the calculated crystalline intensities.

of methanol synthesis over ZrO_2 and Y_2O_3–ZrO_2, Ekerdt and co-workers (2, 3) found evidence of a CO reaction with a Zr cation that has an adjacent O vacancy and an attached bridged OH group. Oxygen vacancies in fluorite-type structure oxide supports, including those created by dopant cations of a lower valency, also play an essential role in the realization of strong metal–support interactions according to the vacancy model put forward by Sanchez and Gazquez (21). At high temperatures oxygen vacancies in the bulk will migrate to the surface that is in contact with the metal. This model elucidates the role of the surface O vacancies ("nests") in anchoring atoms from the metal crystallites to the support, thereby causing them to disperse and react with surrounding gas molecules with enhanced catalytic activity and thermal stability. In view of the defects structure revealed by the present neutron study and the observed improvement in CO removal in Fe catalysis supported by *Ln*–ZrO_2 by Ozawa and Kimura (8), this catalytic system appears to be a good candidate for further investigations of the nature of SMSI phenomena within the vacancy model.

Processing factors, such as the starting materials, agglomeration in the precursor, washing, and heat treatments, are known to markedly influence the texture of the oxide powders prepared by low-temperature techniques (28, 29). Therefore, it is of interest to compare the powder patterns of our high-surface-area pure ZrO_2 with a commercial zirconia powder (from Toso Co., Japan) prepared by high-temperature synthesis. Figure 4 displays the observed and fitted profiles of these two samples. While both the powder patterns are consistent with the well-known monoclinic structure (22, 23), the extreme broadening of the diffraction peaks of the high-surface-area ZrO_2 is caused by the internal strain and small particle incoherency in the powder. The commercial ZrO_2 powder was prepared at high temperature (>900°C), which contains well-grown, submicrometer-size monoclinic particles. In our pure ZrO_2 powder prepared directly from aqueous solution at 100°C followed by a heat treatment at 290°C, very small (<10 nm) microcrystallites were initially formed and subsequently grown to somewhat larger size. Isopropylalchohol was used to wash the product to avoid coalescence between particles during the drying process (18). The micro- and/or mesoporous structure of the powder provides a large effective surface area for the adsorption of hydroxyl groups and water. A detailed neutron-scattering study of the effects of heat treatments on the texture of these zirconia powders will be given in another publication. Our diffraction results suggest that the surface chemistry, controlled to a large extent by the chemisorbed hydroxyl groups and physisorbed water molecules, are quite sensitive to the underlying crystal structure, defects, and texture parameters. This feature can be seen in the dynamics of the adsorbed hydrogen species in these materials, discussed in the next section.

2. *Hydrogen Vibrational Densities of States*

The incoherent scattering function for lattice and local vibrations (phonons) of atoms in an harmonic solid is given by (30)

$$S(Q,E) = \sum_i \frac{c_i\sigma_i}{m_i} \langle (\mathbf{Q}\cdot\mathbf{e})^2 e^{-2W_i(Q)} \rangle \frac{n(E)+1}{E} F_i(E), \quad [1]$$

where c_i, σ_i, m_i, $\mathbf{e}_i$, $e^{-2W_i(Q)}$, and F_i are the concentration, incoherent scattering cross section, mass, phonon unit-polarization vector, Debye–Waller factor, and partial phonon density of states, respectively, for the *i*th atom. ($\hbar\mathbf{Q}$, E) corresponds to the momentum and energy transfer of the neutron, respectively ($\hbar$ being Planck's constant), and $n(E)$ is the Bose thermal occupational factor. At low temperatures and high energies the thermal factor $n(E) + 1 \cong 1$. The quantity with the angular bracket $\langle ... \rangle$ is averaged over all modes with the energy E and, for polycrystalline materials, this also includes averaging over all $\mathbf{Q}$ directions. The ratios, σ_i/m_i, for Zr, O, and H are 0.0723, 0.265, and 81.7 *b*/amu, respectively, for thermal neutrons. Therefore, the scattering function is particularly sensitive to hydrogen vibrations and effectively provides a measure of the hydrogen vibrational density of states. The scattering function given below was obtained from an average over the Q's corresponding to scattering angles of 4° to 20°. Such low-Q region is needed to avoid significant Doppler broadening of the inelastic features at high-momentum transfers. The unit of energy used here is milli-electron volts. For a comparison with optical data, 1 meV is equivalent to 8.066 cm^{-1}.

Inelastic scattering measurements were performed on the following high-surface-area samples: "dry" powders,

$Nd_{0.1}Zr_{0.9}O_{1.95}$ (44 g, heated at 450°C in air for 3 h) and pure ZrO_2 (45 g, heated at 250°C in vacuum for 2 h); "low" water content powders, a 44-g $Nd_{0.1}Zr_{0.9}O_{1.95}$ with 0.33 g of adsorbed water (0.33/44) and a pure ZrO_2 (0.58/45); a "medium" water content powder, $Nd_{0.1}Zr_{0.9}O_{1.95}$ (1.12/44); and a "high" water content powder, $La_{0.1}Zr_{0.9}O_{1.95}$ (1.8/37.6). If an average of 4.6 H_2O molecules is assumed to cover a fully hydroxylated surface of 100 $Å^2$, as found in silica (31), the adsorbed water in the low-water-content Nd–ZrO_2 and ZrO_2 samples, the medium-water-content Nd–ZrO_2, and high-water-content La–ZrO_2 samples correspond statistically to 0.747, 0.882, 2.54, and 4.46 layers of adsorbed water on the surface, respectively. However, we emphasize that water adsorption on zirconia surfaces in general does not show distinct steps of layer adsorption. For example, the nitrogen adsorption–desorption isotherms of heat-treated Y–ZrO_2 prepared differently by Lecloux *et al.* (32) and by Alvarez and Torralvo (33) both showed evidence of micro- and mesoporosity. Capillary condensation was observed at moderate N partial pressure. Therefore, we expect that initially individual water molecules are attached to distinct surface OH groups. As the coverage increases, the tendency of water toward self-association via hydrogen bonding leads to the formation of cluster species prior to the completion of a monolayer coverage.

Figure 5 shows an overview of the observed scattering functions for all the samples, taken with an incident neutron energy of 600 meV at 15 K. For the dry samples that contain only chemisorbed surface OH groups, there are broad features in the 400 to 500-, ~200-, and <150-meV regions. The hydrogen vibrational density of the dry ZrO_2 is significantly higher than that of the dry Nd–ZrO_2 sample. This reflects the fact that the larger surface area in the pure monoclinic ZrO_2 sample accommodates a substantial increase of OH adsorption. As the coverage of water increases, four bands develop: a librational band at ~80 meV due to intermolecular vibrations of the H_2O molecules, two intramolecular bands, one at ~200 meV due to H–O–H bending and the other at ~430 meV due to O–H stretch, and a combination band at ~506 meV. The low-energy spectra obtained from the 50-meV runs (not shown) exhibit the growth of a peak at ~8 meV with increasing water coverage.

A more detailed analysis of the variation of the O–H stretch vibrations and the combination band with water coverage is shown in Figs. 6 and 7. The spectra were fitted to a sum of multiple Gaussian functions and a linear background. In the dry Nd–ZrO_2 sample (Fig. 6a) the O–H stretch band of the surface hydroxyl groups centers at 453 meV (3654 cm^{-1}) with a width of about 17 meV, which is comparable to the instrumental resolution. In the case of pure ZrO_2 (Fig. 7a), the corresponding O–H stretch energy centers at 459 meV (3702 cm^{-1}) with a width of ~23 meV.

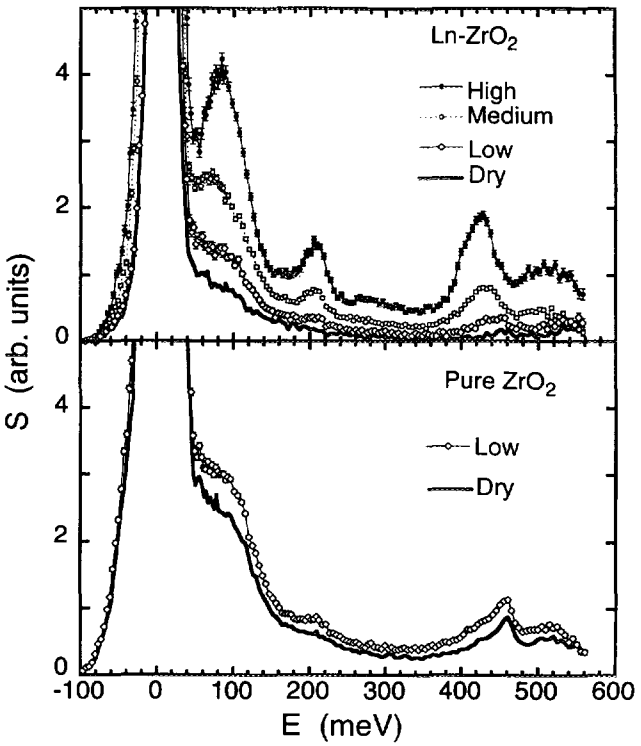

FIG. 5. The observed scattering functions of water adsorbed on Ln–ZrO_2 (top) and pure ZrO_2 (bottom) powders (see text).

In addition, two broad components at about 432 and 510 meV were observed in the dry pure ZrO_2 sample but not in the dry Nd–ZrO_2 sample. These two additional components increase in intensity and become broader in the low-water-content ZrO_2 sample (Fig. 7b). Similar bands also emerge in the low-water Nd–ZrO_2 sample and progressively gain intensity as the water content increases (Figs. 6b–6c). In fact, the spectrum of the high-water sample resembles that of bulk water (34) where the asymmetric stretch bands can be fitted with yet an additional component at ~405 meV (3267 cm^{-1}) (Fig. 6d). In the latter cases where multiple layers or clusters of hydrogen-bonded water molecules are formed, a well-defined H–O–H bending mode and a librational mode at 200 and 80 meV, respectively, were clearly observed (Fig. 5).

The dynamics of adsorbed hydroxyl groups and water molecules provides great value in structural determination of oxide surfaces. We find that the surface hydroxyl stretch vibrations on monoclinic ZrO_2 have a higher energy (3702 cm^{-1}) than those on partially stabilized tetragonal/cubic *Ln*–ZrO_2 (3654 cm^{-1}). The slight broadening of the stretch band indicates that the surface sites available for OH adsorption are more dispersed on the surface of a nominally monoclinic crystal symmetry. Moreover, association among neighboring OH groups to form H_2O-like species would explain the additional components (near 3484 and

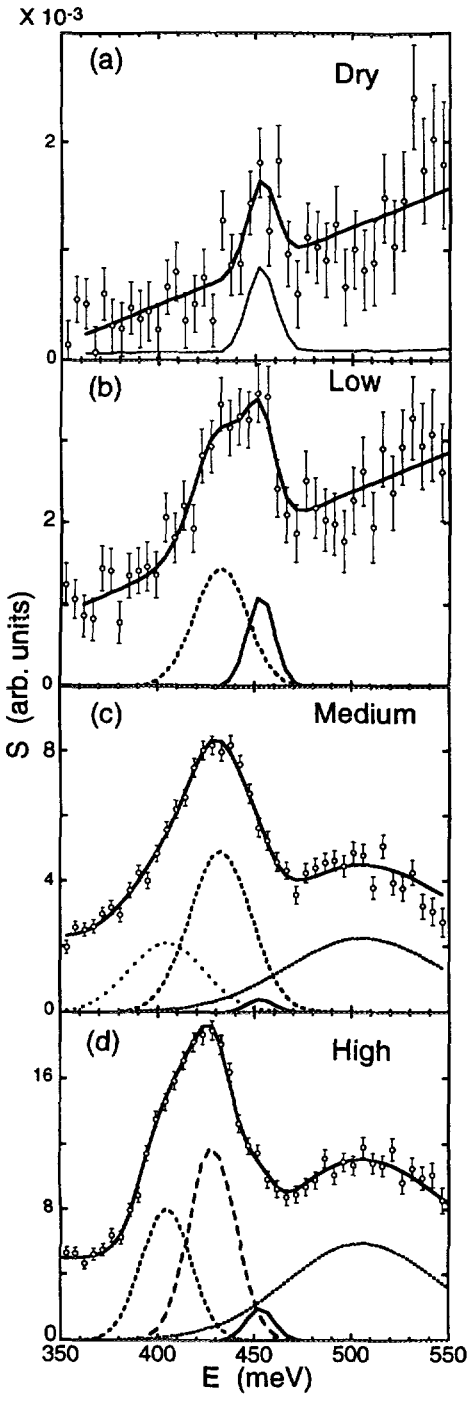

FIG. 6. The O–H stretch vibration band and the combination band fitted to a sum of multiple Gaussian functions and a background for the dry (a), low water content (b), medium water content (c), and high water content (d) samples of lanthanide-modified zirconia.

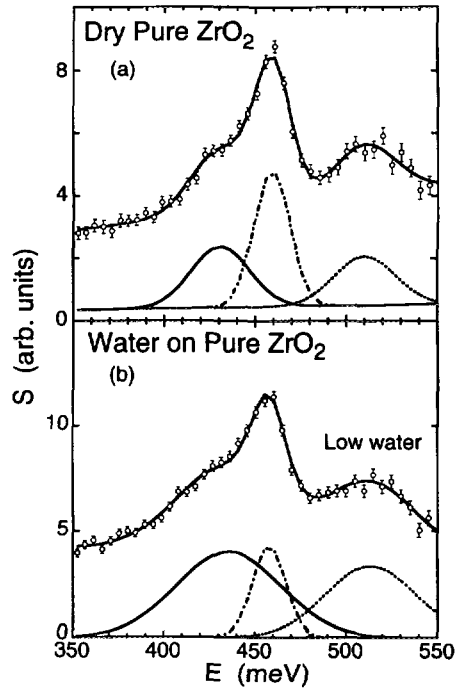

FIG. 7. The O–H stretch vibration band and the combination band fitted to a sum of multiple Gaussian functions and a background for the dry (a) and low water content (b) samples of pure zirconia.

4114 cm^{-1}). Consideration of this different dynamic behavior in conjunction with the different crystal structure and preparation methods for the Ln–ZrO_2 and pure ZrO_2 powders (see preceding section) lends support to the notion that the surface structure and texture of the pure ZrO_2 powder are more complex than the lanthanide-modified ZrO_2 analogs. A previous study (8) also reported marked difference in the catalytic performance in using these two kinds of powders as supports for CO oxidation.

It is of interest to compare the present neutron results with infrared data on similar zirconia systems since both spectroscopic techniques provide useful complementary information (35, 36). Fourier transform infrared spectroscopy (FTIR) is a powerful method for studying catalysis, particularly in probing adsorbed species and surface-related interactions (37–39). The O–H stretch frequencies of absorbed species on various zirconia surfaces have been investigated by many researchers, although the systems studied were not modified by lanthanide doping. Table 2 lists the observed OH stretch frequencies of hydroxyl groups on zirconia reported by various researchers. The IR samples have small surface area (~10 m^2/g), and measurements were carried out at different temperatures among workers (40–52). In general, two characteristic O–H stretch frequencies were found in both monoclinic (m) and tetragonal (t) ZrO_2, such as (m: 3660, 3732; t: 3720, 3827 cm^{-1}) by Erkelens et al. (41); (m: 3660, 3760; t: 3662, 3723 cm^{-1}) by Agron *et al.* (44); and (m: 3700, 3760; t: 3736 cm^{-1}) by Hertl (51). Others reported similar frequency pairs in presumably monoclinic ZrO_2 samples. Attempts were made to assign the two frequencies to termi-

TABLE 2

Stretch Frequencies of Surface OH Groups on Zirconia

Structure	Frequency (cm^{-1})[a]	Surface area (m^2/g)	Heat treatment/ measurement temperatures (K)	Ref.
M	3702 ± 184	106	523/15	This work
T + C[b]	3654 ± 136	~75	723/15	This work
M	3660, 3732		623/623	(41)
T	3720, 3827		623/423	(41)
M	3660, 3760	23.7	773/372	(44)
T	3662, 3725	52.7	773/573	(44)
M	3700, 3760	14	/423	(51)
T	3662, 3725	5	/423	(51)
M	3668, 3780	58	973/298	(48, 50)
M	3670, 3770		773/773	(42)
M	3670, 3770	6–7	773/723	(40)
M	3680, 3780		773/773	(46)
M	3670, 3775	80	723/723	(49)
M	3675, 3740	5.8	473/298	(2)

[a] IR measurements were often made on pressed discs.
[b] Lanthanide-modified zirconia.

nal OH groups where each OH is coordinated to a distinct Zr atom and to bridged OH groups where an OH is coordinated to two Zr atoms. However, the assignments were not consistent among various researchers. (41, 42, 44, 46) Yamaguchi *et al.* (46) suggested that the bridged OH is more stable because of a bidentate configuration. Kondo *et al.* (50) found evidence of stronger CO reaction with the OH groups corresponding to the higher characteristic stretch frequency, and Bensitel *et al.* (49) found that only these OH groups were involved in the reaction with CO_2 to form hydrogenocarbonate. Although the energy shift observed in the *Ln*–ZrO_2 and pure ZrO_2 samples is consistent with the IR data, the present neutron data do not show the two-line structure in the O–H vibrations because of insufficient resolution. The additional components at 405 meV (3266 cm^{-1}) and 432 meV (3527 cm^{-1}) of which the intensities increase with increasing water coverage are definitely the O–H stretch vibration energies of the H_2O molecules, as they were also seen in the IR studies (40–42). In the case of the high-water-content sample, these components sharpen slightly (Fig. 6d), probably resulting from a better organized H-bond network of capillary-condensed water. The effect of hydrogen bonding is evident from the growth of the combination mode at about 510 meV. This feature can be interpreted as breaking of H bonds in the scattering process with a simultaneous excitation of the stretch vibration (53). The association of H_2O molecules also gives rise to the libration and bending modes at 80 and 200 meV, respectively (see Fig. 5).

An *ab initio* calculation using a Hartree–Fock method of an idealized, fully hydroxylated and hydrated (001) surface of tetragonal zirconia has been carried out recently by Orlando *et al.* (54, 55). These authors found that dissociated water (OH group) is by 2.2 kcal/mol more stable than adsorbed water (H_2O) whose adsorption energy is about 15 kcal/mol. This small energy difference suggests the possible coexistence of these two species on a ZrO_2 surface. This situation appears to be the case in our pure ZrO_2 sample. The bridged hydroxyl group was found to be energetically more favorable than the terminal configuration. The O–H stretch vibrational frequencies for these two OH group configurations were calculated to be separated by more than 300 cm^{-1}, which disagrees with the experimental results. The binding properties of hydroxyl species on zirconia and their relationship to catalytic performance are complex phenomena. Clearly, more experimental and theoretical studies are needed for a better understanding of this important issue.

IV. CONCLUSIONS

Selected samples of high-surface-area pure zirconia and lanthanide-modified zirconia were studied by neutron spectroscopy. The crystal phases of the zirconia powders and the hydrogen vibrational densities of states of the adsorbed hydroxyl species on the surface of these powders were characterized. Using neutron powder diffraction and a Rietveld analysis the crystal structure of the heat-treated $La_{0.1}Zr_{0.9}O_{1.95}$ and $Nd_{0.1}Zr_{0.9}O_{1.95}$ samples was determined to be a composition of tetragonal and cubic phases. The result was compared with the monoclinic structure of pure zirconia. As expected, preservation of electroneutrality in the lanthanide-doped zirconia lattice results in oxygen-vacancy-induced defects. A Fourier filtering technique was employed to examine the short-range defects structure in $La_{0.1}Zr_{0.9}O_{1.95}$ and $Nd_{0.1}Zr_{0.9}O_{1.95}$. We obtained a real-space correlation function that shows evidence of static atomic displacement along the pseudocubic ⟨111⟩ and other directions, probably due to relaxation of atoms near the oxygen vacancies. Oxygen vacancy sites surrounded by relaxed atoms in the present fluorite-type structure Ln–ZrO_2 samples may play an important role in OH and H_2O adsorption during methanol synthesis and in the water–gas shift reaction. The powder pattern of a high-surface-area monoclinic ZrO_2, on the other hand, showed extreme broadening of the diffraction peaks due to texture introduced by the low-temperature synthesis. The hydrogen densities of states of adsorbed OH groups and water on *Ln*–ZrO_2 and in pure ZrO_2 were measured over an energy range from 0 to 550 meV (0–4440 cm^{-1}). The vibrational frequencies characteristic of O–H stretch vibrations as well as inter- and intramolecular vibrations of H_2O were monitored from submonolayer coverage to capillary condensation of water. The neutron results were compared with infrared data from similar zirconia systems and *ab initio* calculations found in the literature.

ACKNOWLEDGMENTS

We thank Dr. Mareo Kimura (Toyota Research and Development Laboratory) for his help in sample preparation and Dr. Lennox Iton (Argonne) for helpful discussion. Work performed at the Argonne National Laboratory is supported by the U.S. DOE-BES under Contract No. W-31-109-ENG-38.

REFERENCES

1. Nakano, Y., Iizuka, T., Hattori, H., and Tanabe, K., *J. Catal.* **57,** 1 (1979).
2. He, M.-Y., and Ekerdt, J. G., *J. Catal.* **87,** 238 (1984), **87,** 381 (1984), and **90,** 17 (1984).
3. Jackson, N. B., and Ekerdt, J. G., *J. Catal.* **101,** 90 (1986), **126,** 31 (1990), and **126,** 46 (1990).
4. Tseng, S. C., Jackson, N. B., and Ekerdt, J. G., *J. Catal.* **109,** 284 (1988).
5. Silver, R. G., Hou, C. J., and Ekerdt, J. G., *J. Catal.* **118,** 400 (1989).
6. Kuno, H., Takahashi, K., Shibagaki, M., Shimazaki, K., and Matsushita, H., *Bull. Chem. Soc. Jpn.* **63,** 1943 (1990).
7. Miyoshi, N., Matsumoto, S., Ozawa, M., and Kimura, M., Society of Automotive Eng., Technical paper series 891970, 1989.
8. Ozawa, M., and Kimura, M., *J. Less-Common Met.* **171,** 195 (1991).
9. Matsumoto, S., Miyoshi, N., Kanazawa, T., Kimura, M., and Ozawa M., *in* "Catalytic Science and Technology" (S. Yoshida, N. Takezawa, and T. Ono, Eds.), Vol. 1, p. 335. Kodansha, Tokyo, 1991.
10. Ozawa, M., Kimura, M., and Isogai, A., *J. Alloys Compounds* **193,** 73 (1993); and United States Patent No. 5,075,276 (1991).
11. Barbier, Jr., J., and Duprez, D., *Appl. Catal. B* **4,** 105 (1994) and references therein.
12. Jorgensen, J. D., Faber, Jr., J., Carpenter, J. M., Crawford, R. K., Haumann, J. R., Hitterman, R. L. Kleb, R., Ostrowski, G. E., Rotella, F. J., and Worton, T. G., *J. Appl. Crystallogr.* **22,** 321 (1989).
13. Rietveld, H. W., *J. Appl. Crystallogr.* **2,** 65 (1968).
14. Richardson, Jr., J. W., and Faber, Jr., J., *Adv. X-Ray Anal.* **29,** 143 (1985).
15. Loong, C.-K., Ikeda, S., and Carpenter, J. M., *Nucl. Instrum. Meth. A* **260,** 381 (1987).
16. Green, D. J., Hannink, R. H. J., and Swain, M. V., "Transformation Toughening of Ceramics." CRC Press, Boca Raton, FL, 1989.
17. Withers, R. L., Thompson, J. G., and Barlow, P. L., *J. Solid State Chem.* **94,** 89 (1991).
18. Kaliszewski, M. S., and Heuer, A. H., *J. Am. Ceram. Soc.* **73,** 1504 (1990).
19. Yoshimura, M., *Ceram. Bull.* **67,** 1950 (1988).
20. Ozawa, M., Suzuki, S., and Loong, C.-K., *J. Mater. Sci. Lett.* **14,** 796 (1995).
21. Sanchez, M. G., and Gazquez, J. L., *J. Catal.* **104,** 120 (1987).
22. Brown, F. H., and Duwez, P., *J. Am. Ceram. Soc.* **38,** 95 (1955).
23. Bastide, B., Odier, P., and Coutures, J. P., *J. Am. Ceram. Soc.* **71,** 449 (1988).
24. Loong, C.-K., Richardson, Jr., J. W., Ozawa, M., and Kimura, M., *J. Alloys Compounds* **207/208,** 174 (1994).
25. The mole-fraction, microstrain, and crystallite-size parameters for the cubic and tetragonal phases given in Table 1 were obtained from a self-consistent analysis of the data and their correlations in the fit were examined carefully. Thus the mole fractions should be regarded to be more accurate than those reported previously in Ref. (24).
26. Larson, A. C., and Von Dreele, R. B., "Generalized Structural Analysis System." Los Alamos Report LAUR 86-748, 1987.
27. Warren, B. E., and Averbach, B. L., *J. Appl. Phys.* **21,** 595 (1950).
28. Schwarz, J. A., Contescu, C., and Jagiello, J., *Catalysis* **11,** 127 (1994).
29. Rijnten, H. Th., *in* "Physical and Chemical Aspects of Adsorbents and Catalysts" (B. G. Linsen, Ed.) p. 315. Academic Press, New York, 1970.
30. Price, D. L., and Sköld, K., *in* "Neutron Scattering" (K. Sköld and D. L. Price, Eds.), Vol. A, Chap. 1, p. 29. Academic Press, Orlando, 1986.
31. Knözinger, H., *in* "The Hydrogen Bond—Recent Developments in Theory and Experiments" (P. Schuster, G. Zundel, and C. Sandorfy, Eds.), p. 1263. North-Holland, Amsterdam, 1976.
32. Lecloux, A. J., Blacher, S., Kessels, P.-Y., Marchot, P., Merlo, J.-L., Noville, F., and Pirard, J.-P., *in* "Characterization of Porous Solids II (F. Rodríguez-Reinoso, J. Rouquerol, K. S. W. Sing, and K. K. Unger, Eds.), p. 659. Elsevier, Amsterdam, 1991.
33. Alvarez, M. R., and Torralvo, M. J., *Colloids Surf. A* **83,** 175 (1994).
34. Toukan, K., Ricci, M. A., Chen, S.-H., Loong, C.-K., Price, D. L., and Teixerira, J., *Phys. Rev. A* **37** (1988) 2580.
35. Cavanagh, R. R., Rush, J. J., Kelley, R. D., and Udovic, U., *J. Chem. Phys.* **80,** 3478 (1984).
36. Eckert, J., *Physica B + C* **136,** 150 (1986).
37. Angell, C. L., *in* "Fourier Transform Infrared Spectroscopy" (J. R. Ferraro and L. J. Basile, Eds.), Vol. 3, p. 1. Academic Press, New York, 1982.
38. Little, L. H., "Infrared Spectra of Adsorbed Species." Academic Press, New York, 1966.
39. Hair, M. L., "Infrared Spectroscopy in Surface Chemistry." Dekker, New York, 1967.
40. Tret'yakov, N. E., Pozdnyakov, D. V., Oranskaya, O. M., and Filimonov, V. N., *Russ. J. Phys. Chem.* **44,** 596 (1970).
41. Erkelens, J., Rijnten, H. Th., and Eggink-du Burck, S. H., *Recueil* **91,** 1426 (1972).
42. Tsyganenko, A. A., and Filimonov, V. N., *J. Mol. Struct.* **19,** 579 (1973).
43. Yamaguchi, T., Sasaki, H., and Tanabe, K., *Chem. Lett.*, 1017 (1973).
44. Agron, P. A., Fuller, Jr., E. L., and Holms, H. F., *J. Colloid Interface Sci.* **52,** 553 (1975).
45. Yamaguchi, T., Nakano, Y., Iisuka, T., and Tanabe, K., *Chem. Lett.*, 677 (1976).
46. Yamaguchi, T., Nakano, Y., and Tanabe, K., *Bull. Chem. Soc. Jpn.* **51,** 2482 (1978).
47. Edwards, J. F., and Schrader, G. L., *J. Catal.* **94,** 175 (1985).
48. Onishi, T., Abe, H., Maruya, K., and Domen, K., *J. Chem. Soc. Chem. Commun.*, 617 (1985), 103 (1986).
49. Bensitel, M., Moravek, V., Lamotte, J., Saur, O., and Lavalley, J. C., *Spectrosc. Acta A* **43,** 1487 (1987).
50. Kondo, J., Abe, H., Sakata, Y., Maruya, K., Domen, K., and Onishi, T., *J. Chem. Soc. Faraday Trans.* **84,** 511 (1988).
51. Hertl, W., *Langmuir* **5,** 96 (1989).
52. Kondo, J., Sakata, Y., Domen, K., Maruya, K., and Onishi, T., *J. Chem. Soc. Faraday Trans.* **86,** 397 (1990).
53. Riccci, M. A., Chen, S.-H., Price, D. L., Loong, C.-K., Toukan, K., and Teixeira, J., *Physica B* **136,** 190 (1986).
54. Orlando, R., Pisani, C., Roetti, C., and Stefanovich, E., *Phys. Rev. B* **45,** 592 (1992).
55. Orlando, R., Pisani, C., Ruiz, E., and Sautet, P., *Surf. Sci.* **275,** 482 (1992).